ACS APPLIED MATERIALS & INTERFACES

Research Article

www.acsami.org

Multilayer-Coated Liquid Crystalline Nanoparticles for Effective Sorafenib Delivery to Hepatocellular Carcinoma

Raj Kumar Thapa,[†] Ju Yeon Choi,[†] Bijay K. Poudel,[†] Tran Tuan Hiep,[†] Shiva Pathak,[†] Biki Gupta,[†] Han-Gon Choi,[*,‡] Chul Soon Yong,[*,†] and Jong Oh Kim[*,†]

[†]College of Pharmacy, Yeungnam University, 280 Daehak-Ro, Gyeongsan, Gyeongsanbuk-do 712-749, South Korea

[‡]College of Pharmacy, Hanyang University, 55, Hanyangdaehak-ro, Sangnok-gu, Ansan 426-791, South Korea

Supporting Information

ABSTRACT: Hepatocellular carcinoma is one of the most common cancers in adults and develops due to activation of oncogenes and inactivation of tumor suppressor genes. Sorafenib (SF) is a U.S. Food and Drug Administration (FDA) approved drug for the treatment of hepatocellular carcinoma. However, its clinical use is limited by its poor aqueous solubility and undesirable side effects. Monoolein-based liquid crystalline nanoparticles (LCN) are self-assembled structures that have been determined as promising drug-delivery vehicles. Therefore, the main aim of this study was to prepare layer-by-layer (LbL) polymer-assembled SF-loaded LCNs (LbL-LCN/SF) for effective delivery of SF to hepatocellular carcinoma. Results revealed that LbL-LCN/SF presented optimum particle size (~165 nm) and polydispersity index (PDI, ~0.14) with appropriate polymer layer assembly confirmed by transmission electron microscopy (TEM) and atomic force microscopy (AFM). Furthermore, LbL-LCN/SF effectively controlled burst release and exhibited pH-sensitive release of SF, thereby increasing drug release in the acidic microenvironment of tumor cells. Compared to free SF and bare LCN, the hemolytic activity of LbL-LCN/SF was significantly reduced ($p < 0.01$). Interestingly, LbL-LCN/SF was more cytotoxic to HepG2 cells than the free drug was. Additionally, high cellular uptake and greater apoptotic effects of LbL-LCN/SF in HepG2 cells indicates superior antitumor effects. Therefore, LbL-LCN/SF is a potentially effective formulation for hepatocellular carcinoma.

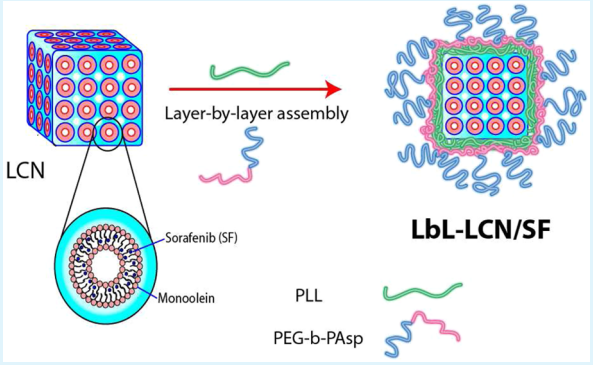

KEYWORDS: *liquid crystalline nanoparticles, sorafenib, hepatocellular carcinoma, multilayer, layer-by-layer*

INTRODUCTION

Cancer is one of the leading causes of death in both developed and developing countries.[1] Every year, more than a half-million people worldwide are diagnosed with hepatocellular carcinoma including approximately 20,000 new cases in the U.S. alone. Liver cancer is the fifth most common cancer in men and seventh in women.[2] Hepatocellular carcinoma develops in a stepwise process involving activation of oncogenes and inactivation of tumor suppressor genes leading to overactivation of Raf/MEK/extracellular signal-regulated kinase (ERK).[3−5]

Sorafenib (SF) is the first drug approved by the U.S. Food and Drug Administration (FDA) for the systemic treatment of patients with advanced hepatocellular carcinoma refractory to treatment with liver transplantation or surgical resectioning. It is a biaryl urea, which inhibits serine/threonine isoforms (such as Raf-1 and B-Raf) and, thereby, blocks the Raf/MEK/ERK pathway. In addition, it inhibits upstream receptor tyrosine kinases, which play an important role in angiogenesis including vascular endothelial growth factor receptor (VEGFR)-2, VEGFR-3, and Kit.[6] However, various problems including poor aqueous solubility and undesirable side effects limit its clinical application. The major side effects of sorafenib treatment are elevated blood pressure, diarrhea, fatigue, hand−foot syndrome, skin rash/desquamation, and nausea.[6,7] These side effects might be overcome by the use of nanoparticles that can control and target the release of SF to the specific tumor site.[8,9]

Nanoparticles are one of the most widely investigated site-targeted drug-delivery carriers, and in the past few years, liquid crystalline nanoparticles (LCN) have been identified as promising drug-delivery vehicles. LCN are self-assembled structures formed on exposure of polar lipids (such as monoolein) to polar environments in the presence of suitable surfactants. These assembled particles consist of nonlamellar structures with hydrophilic and lipophilic domains.[10] The self-assembly of the lipids provides both rigidity and fluidity, leading to higher stability, sustained drug release, and high drug payload to the target site.[11,12]

Received: July 10, 2015
Accepted: August 28, 2015
Published: August 28, 2015

DOI: 10.1021/acsami.5b06203
ACS Appl. Mater. Interfaces 2015, 7, 20360−20368

The intravenous administration of LCNs as nanocarrier systems would be effective in targeted drug delivery to tumor sites. However, there are some problems associated with the direct intravenous administration of LCNs including its bioadhesivity, which might lead to LCNs binding to non-targeted sites such as blood vessel walls. Another problem is its rapid removal from the blood circulation. Furthermore, the toxicity of LCN might induce excessive hemolysis.[13] In order to solve these problems, we developed a polymer-coated LCN with layers of poly-L-lysine (PLL) and poly(ethylene glycol)-*b*-poly(aspartic acid) (PEG-*b*-PAsp). PEGylated carriers demonstrate attractive characteristics including controlled drug release, targeted delivery, and improved therapeutic indices of anticancer activities.[14] It is a well-known fact that PEGylation imparts stealth effects and, thereby, prevents immune recognition of drug carrier and subsequent clearance from the body.[15] Different layers of polymer coating further control drug release, protect from possible enzymatic attack, and enhance drug stability.

The present study focuses on the preparation of SF-loaded LCNs (LbL-LCN/SF) coated with up to six layers of PLL and PEG-*b*-PAsp, to enhance SF delivery to hepatocellular carcinoma cells. For this purpose, different additives and processing parameters were optimized, and polymer coating with outer PEG layers was performed to make the LCNs more hemocompatible and maintain the sustained release characteristics. LbL-LCN was characterized, and cellular uptake, as well as cytotoxic potential, was studied in a hepatocellular carcinoma cell line.

EXPERIMENTAL METHODS

Materials. Sorafenib was purchased from Green Stone Swiss Co., Ltd., (Fujian, China). Monoolein was a kind gift from Danisco Co., Ltd., (Tokyo, Japan). Poloxamer 407 was purchased from BASF (Ludwigshafen, Germany). PLL (MW 15000−30000) and coumarin-6 were purchased from Sigma-Aldrich (St Louis, MO, USA). PEG-*b*-PAsp (MW 6400) was purchased from Alamanda Polymers (Huntsville, AL, USA) and LysoTracker Red was purchased from Thermo Fischer Scientific Inc., (Waltham, MA, USA). Human hepatocellular carcinoma (HepG2) cells were obtained from the Korean Cell Line Bank (Seoul, South Korea). All other chemicals were of reagent grade and used without further purification.

Fabrication of Layer-by-Layer Polymer-Assembled LCN/SF (LbL-LCN/SF). We prepared optimal LbL-LCN/SF by first optimizing the LCN formulation using a previously reported method with slight modifications.[16,17] Briefly, the hydrophobic phase (monoolein and poloxamer 407) was melted at 60 °C in a vial followed by mixing with SF. Ethanol was added to the mixture of monoolein, poloxamer 407 and sorafenib, followed by vortexing to mix properly. Simultaneously, the required amount of PVA was added to hot distilled water, mixed to dissolve and allowed to cool for addition in further steps as the aqueous phase. Then, this aqueous phase was added followed by vortexing for 30 s and probe sonication for 10 min (at 70% amplitude) to obtain the LCN formulation (LCN/SF). Different quantities of monoolein, poloxamer 407, poly(vinyl alcohol) (PVA), and ethanol were tested to determine the appropriate concentration for the preparation of the optimum LCN formulation. SF concentration in the formulation was optimized by determining its entrapment efficiency (EE) and loading capacity (LC) in the LCNs.

Next, LbL-LCN/SF was prepared using slight modifications of a previously described method.[18] A small aliquot of polymer solution (PLL or PEG-*b*-PAsp) was added to the LCN/SF solution and vortexed followed by sonication for 5 min, and the mixture was kept for further polymer addition in subsequent steps. The appropriate amount of polymer required for charge reversal was determined by careful titration.

Hydrodynamic Particle Size, Polydispersity, and ζ Potential Analysis. Particle size, polydispersity index (PDI), and ζ potential were measured using dynamic light scattering (DLS) with a Nano-S90 ZetaSizer (Malvern Instruments, Worcestershire, U.K.). Following measurements, the final particle size was determined using the Stokes−Einstein equation while ζ potential and PDI were determined using Nano DTS software (version 6.34). All measurements were performed at 25 °C with at least three sets of 10 runs.

Transmission Electron Microscopy. The cross-sectional morphology of LCN/SF and LbL-LCN/SF was examined using transmission electron microscopy (TEM, H7600, Hitachi, Tokyo, Japan). Briefly, the formulation was mixed with phosphotungstic acid, placed on a carbon-coated copper grid, and then dried under infrared radiation. The grid was then viewed under the accelerating voltage using a microscope.

Atomic Force Microscopy. LCN/SF and LbL-LCN/SF were adsorbed on mica squares and air-dried to remove excess water. Atomic force microscopy (AFM) analysis was performed using a Nanoscope IIIa scanning probe microscope (Digital Instruments, Murray Hill, NJ, USA) operating at tapping mode with a commercial pyramidal silicon tip with a radius of 10 nm and a nominal force constant of 0.1 N/m. The amplitude signal of the cantilever in the trace direction and height signal in the retrace direction were simultaneously displayed on the images to demonstrate the exact morphology of the LCN/SF and LbL-LCN/SF.

Fourier Transform Infrared Spectroscopy Analysis. LCN/SF and LbL-LCN/SF were characterized by Fourier transform infrared (FTIR) using a Thermo Scientific Nicolet Nexus 670 FTIR spectrometer and Smart iTR with a diamond window (Thermo Fischer Scientific). The samples were placed on the machine, and the spectra were recorded over the range of 550−4000 cm^{-1}.

Differential Scanning Calorimetric Analysis. The thermal behavior of monoolein, poloxamer 407, SF, LCN/SF, and LbL-LCN/SF were studied using a Q200 calorimeter (TA Instruments, New Castle, DE, USA). LCN/SF and LbL-LCN/SF formulations were freeze-dried prior to analysis. Samples were placed in compact aluminum pans and gradually heated from 0 to 270 °C, at a rate of 10 °C/min to obtain the respective thermograms.

Determination of EE. SF entrapment in LCN/SF and LbL-LCN/SF was calculated by determining the free and total drug concentrations in the formulations. Briefly, LbL-LCN formulations were filtered using an Amicon centrifugal ultrafiltration device (MWCO 10000 Da; Millipore, Billerica, MA, USA) for 10 min at 5000 rpm. SF concentration was determined using a high-performance liquid chromatography (HPLC) system (Hitachi, Tokyo, Japan) that was comprised of an L-2130 pump, L-2200 autosampler, L-2420 ultraviolet−visible (UV−vis) detector, and L-2350 column oven with Ezchrom elite software (version 318a). An Inertsil C_{18} column (150 mm × 4.6 mm; 5-μm particle size; Cosmosil, Nacalai Tesque Inc., San Diego, CA, USA) was used to perform isocratic elution with a mobile phase consisting of methanol:acetonitrile:acetic acid (1%) at a ratio of 38:35:27 (v/v/v), flow rate of 1.0 mL/min, and column temperature of 37 °C. A sample of 20 μL was injected for each analysis, and UV absorbance was measured at a wavelength of 254 nm. The EE (%) was determined using the following formula:

$$\mathrm{EE}/\% = \frac{W_{\mathrm{LCN}}}{W_{\mathrm{T}}} \times 100$$

where W_{LCN} = weight of SF entrapped in LCN and W_{T} = total SF added to the LCN formulation.

Similarly, the LC (%) was determined using the following formula:

$$\mathrm{LC}/\% = \frac{W_{\mathrm{TD}} - W_{\mathrm{UD}}}{W_{\mathrm{TL}}} \times 100$$

where W_{TD}, W_{UD}, and W_{TL} are weights of the total drug, unbound drug, and total lipid, respectively.

In Vitro Drug Release. The release of SF from LCN/SF and LbL-LCN/SF was assessed using a dialysis method. Aliquots of LCN/SF and LbL-LCN/SF were placed in the dialysis membrane tubing

DOI: 10.1021/acsami.5b06203
ACS Appl. Mater. Interfaces 2015, 7, 20360−20368

(Spectra/Por; MWCO 3500 Da, SpectrumLabs, Rancho Dominguez, CA, USA) and immersed in 30 mL of phosphate-buffered saline (PBS, 0.01 M, pH 7.4 or 0.01 M, pH 5.5) containing 0.1% (v/v) Tween 80 to maintain a sink condition. At predetermined intervals, samples were withdrawn and replaced with fresh medium maintained at 37 °C. Finally, the concentration of SF in the release medium was quantified using a HPLC method as described previously.

Hemolytic Toxicity Analysis. The hemolytic toxicity study was performed using previously reported procedures with slight modifications.[19,20] Briefly, fresh whole blood from male Sprague–Dawley (SD) albino rats was collected and centrifuged at 2000 rpm for 15 min in an ultracentrifuge. The RBCs were collected, washed with physiological saline to obtain a clear colorless supernatant above the cell mass, resuspended in normal saline to obtain 2% erythrocyte concentration, and then used for the hemolytic toxicity study. The negative control consisted of 1 mL each of RBC suspension and physiological saline while the saline was replaced with 1% Triton X 100 for the positive control (i.e., 100% hemolytic). Different concentrations of the free SF, blank LCN, LCN/SF, and LbL-LCN/SF were mixed with equal volumes of RBC and incubated at 37 ± 0.5 °C for 1 h. Following incubation, the samples were centrifuged at 1500 rpm for 10 min, and then hemoglobin contents of the supernatants were quantified spectrophotometrically at λ_{max} 540 nm against the control. Percentage hemolysis was calculated using the following formula:

$$\text{hemolysis}/\% = \frac{A_S - A_{NC}}{A_{PC} - A_{NC}} \times 100$$

where A_S, A_{PC}, and A_{NC} are the absorbance values of the sample and positive and negative controls, respectively.

In Vitro Cytotoxicity Study. The in vitro cytotoxicity of free SF, blank LbL-LCN, and LbL-LCN/SF were assessed using a 3-(4,5-dimethylthiazol-2-yl)-5-(3-carboxymethoxyphenyl)-2-(4-sulfophenyl)-2*H*-tetrazolium (MTS) assay (Promega, Madison, WI, USA). HepG2 cells were seeded in 96-well plates at a density of 1×10^4 cells/well and incubated for 24 h. Cells were treated with different concentrations of free SF, blank LbL-LCN, and LbL-LCN/SF, incubated for a further 24, 48, and 72 h, washed twice with PBS, and then treated with MTS solution. Untreated cells served as the control, and absorbance was measured at 493 nm using an automated microplate reader.

Intracellular Uptake Study. HepG2 cells were seeded in coverslips placed in 12-well plates at a density of 2×10^4 cells/well, incubated for 24 h, and coumarin-6-loaded LbL-LCNs were added to each well followed by a 30 min incubation. Then, LysoTracker Red was added to each well with an additional 10 min incubation. The final concentrations of coumarin-6 and LysoTracker Red were 1 μg/mL and 100 ng/mL, respectively. The cells were then washed with PBS, fixed with 4% paraformaldehyde solution in the dark, and finally washed with PBS. The coverslips were mounted on glass slides, sealed with glycerin, and observed using confocal laser scanning microscopy (CLSM, Leica Microsystems, Wetzlar, Germany).

In addition, HepG2 cells were seeded at a density of 1×10^5 cells/well in a 12-well plate, incubated for 24 h, and treated with coumarin-6-loaded LbL-LCNs at a concentration of 1 μg/mL in a humidified incubator with 5% CO_2 atmosphere at 37 °C. After incubation for 30 min, cells were washed with PBS, harvested, and finally dispersed in 1.5 mL of PBS for flow cytometric analysis using a fluorescence-activated cell sorting (FACS) Calibur flow cytometer (BD Biosciences, San Jose, CA, USA).

Apoptosis Assay. HepG2 cells were seeded at a density of 1×10^5 cells/well in a 12-well plate and incubated for 24 h. Then, they were treated with free SF and LbL-LCN/SF for 24 h. Afterward, cells were harvested, washed with PBS, collected, mixed with binding buffer, and then stained with Annexin-V and PI for 10 min in the dark. Finally, the cells were diluted with binding buffer and analyzed for apoptosis using a FACS Calibur flow cytometer.

Statistical Analysis. The results are presented as mean ± standard deviation (SD). The Student's *t*-test was used to determine the level of statistical significance between the groups, and $p < 0.05$ was considered statistically significant.

RESULTS AND DISCUSSION

Preparation of LbL-LCN/SF. Figure 1 illustrates the fabrication process for LbL-LCN/SF. The preparation involved

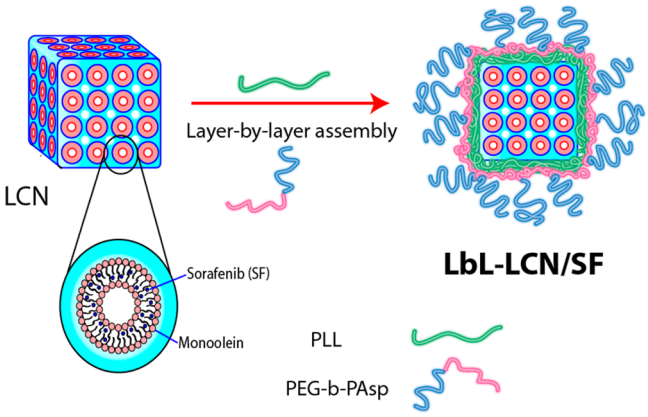

Figure 1. Schematic representation of fabrication of layer-by-layer polymer-assembled sorafenib-loaded liquid crystalline nanoparticles (LbL-LCN/SF).

melting and mixing of the hydrophobic phase (monoolein, poloxamer 407, and SF) followed by addition of the aqueous phase and probe sonication. The LCN/SF was then coated with three alternate layers of PLL and PEG-*b*-PAsp to obtain the final PEGylated LbL-LCN/SF. It is a well-known fact that PEGylated nanoparticles < 200 nm in size enhanced the permeation and retention effect (EPR) that passively targets drugs to tumor tissues.[21,22] In addition, it facilitates their invasion of the reticuloendothelial system based on systemic clearance.[21,22] Therefore, the final formulation was optimized using different proportions of additives, to obtain appropriately sized nanoparticles.

The LCN formulations were first optimized for appropriate amounts of monoolein/poloxamer 407, PVA, ethanol, and SF. Figure S1A shows the effect of different ratios of monoolein and poloxamer 407 on particle size and ζ potential of LCNs. A reduction in the quantity of monoolein reduced the particle size of the LCNs while a monoolein/poloxamer 407 ratio of 80:20 produced LCNs with the lowest particle size, PDI, and appropriate ζ potential. Poloxamer ratios above this cannot be used because only proportions of up to 20% (w/w) monoolein can form LCNs.[17] The effect of PVA on LCNs was determined as shown in Figure S1B, and no significant change was observed in the particle size of the LCNs. However, PDI was the lowest with 1% PVA, suggesting that a superior stabilizing effect was obtained with PVA at this concentration. Furthermore, the stabilizing effect of PVA facilitates maintenance of the LCN phase and prevents phase inversion.[23] Ethanol was used as hydrotrope to aid in the optimization of LCNs prepared with monoolein and poloxamer (80:20) and PVA (1%, Figure S1C). The concentration of ethanol was varied at a range of 0–4% (w/w) with respect to the dispersed phase. A decreasing particle size and PDI were observed with increasing amounts of ethanol, and lowest values were observed with 4% ethanol. At appropriate concentrations, ethanol acts as a hydrotrope and, therefore, can be used to disperse and solubilize monoolein in an aqueous system.[24]

DOI: 10.1021/acsami.5b06203
ACS Appl. Mater. Interfaces 2015, 7, 20360–20368

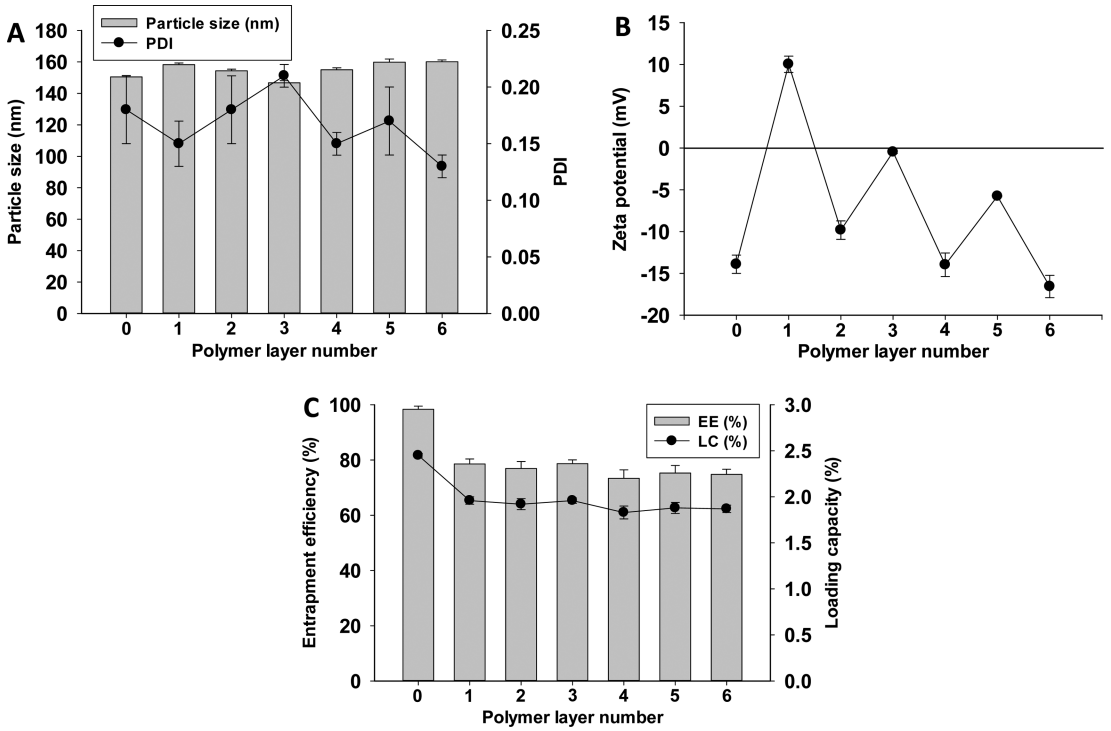

Figure 2. Effect of polymer layer assembly on (A) particle size and polydispersity index (PDI), (B) ζ potential of sorafenib-loaded liquid crystalline nanoparticles (LCN/SF), and (C) entrapment efficiency (EE) and loading capacity (LC) of LCN/SF. Data are expressed as mean ± SD; n = 3.

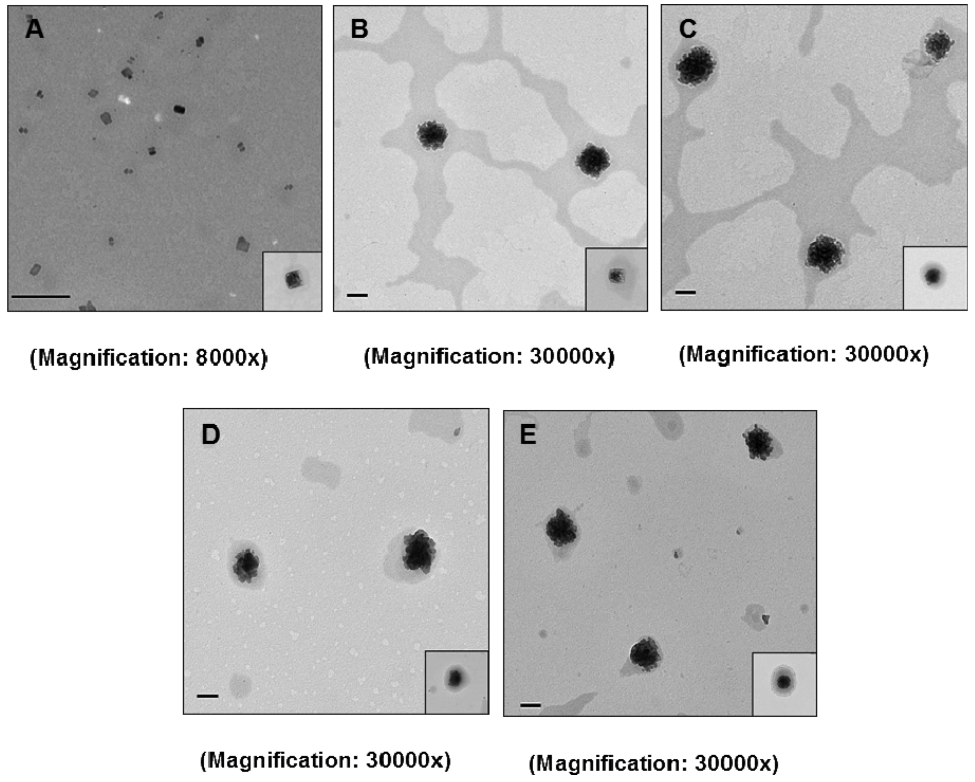

Figure 3. Transmission electron microscopy (TEM) images of (A and B) sorafenib-loaded liquid crystalline nanoparticles (LCN/SF), (C) two-layered LCN/SF, (D) four-layered LCN/SF, and (E) six-layered layer-by-layer polymer-assembled LCN/SF (LbL-LCN/SF). Scale bar, images A and B−D, 500 and 100 nm, respectively.

SF, as an active pharmaceutical ingredient, was incorporated in the nanoparticles. SF is hydrophobic in nature and, therefore, can be incorporated into the hydrophobic core of the LCNs.[8] We found that increasing the amount of SF in the LCN formulation subsequently increased the particle size (Figure S2A). PDI was found to be below 0.3 at SF concentrations of up to 2.5%, but, above this level, we observed an abrupt increase in PDI, suggesting polydispersion of LCNs. This

DOI: 10.1021/acsami.5b06203
ACS Appl. Mater. Interfaces 2015, 7, 20360−20368

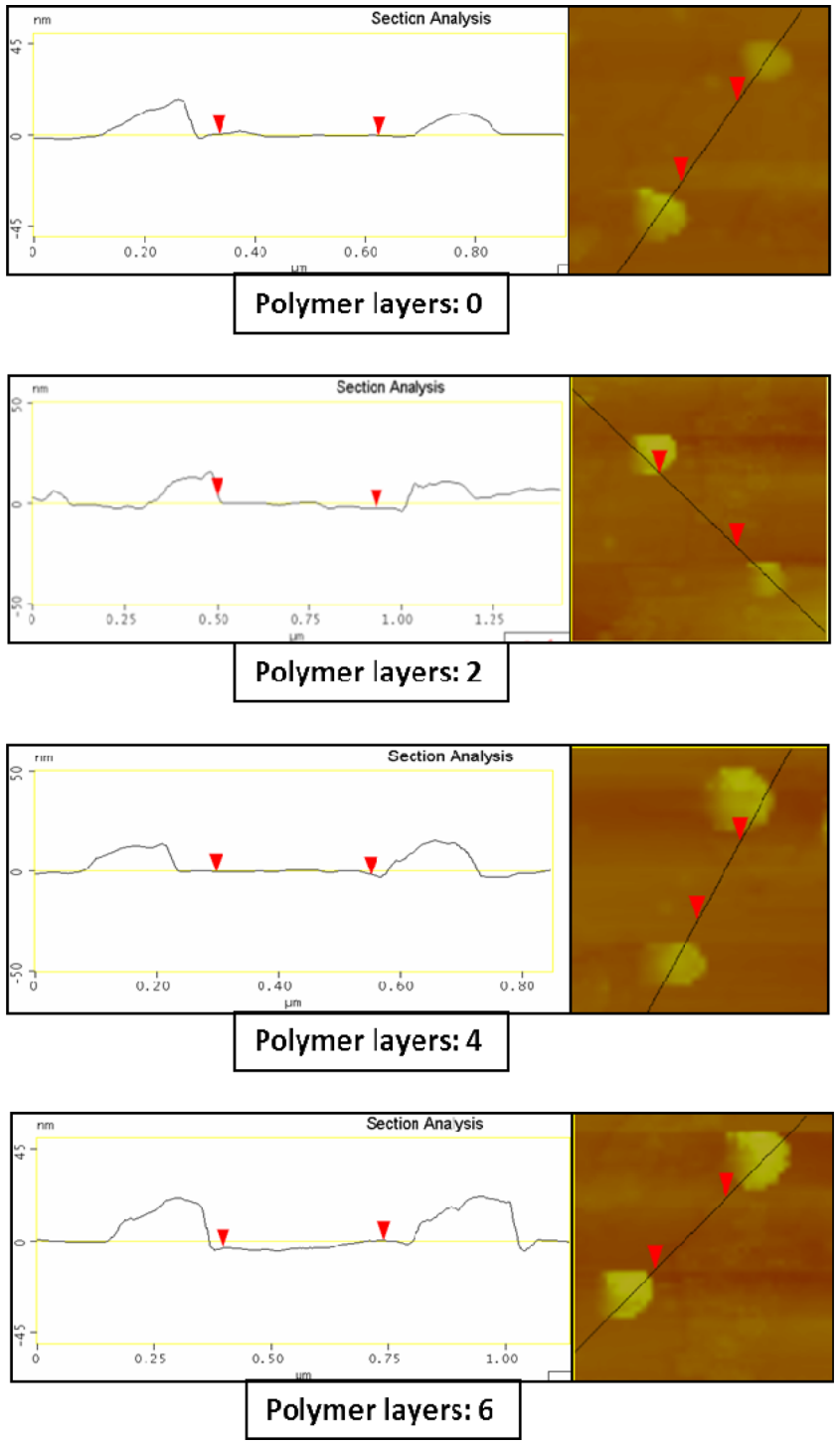

Figure 4. Atomic force microscopy (AFM) images of sorafenib-loaded liquid crystalline nanoparticles (LCN/SF) and layer-by-layer polymer-assembled (LbL)-LCN/SFs.

phenomenon might be attributable to the enhanced incorporation of SF in LCNs, which increased the particle size. The effect of different quantities of SF on the EE and LC is presented in Figure S2B. At the chosen SF concentration (2.5% (w/w) monoolein), the EE and LC were almost 100 and about 2.5%, respectively.

Layer-by-layer polymer assembly of the LCN/SF was then performed to enhance biocompatibility and reduce toxicity, by PEGylation. PLL and PEG-*b*-PAsp were used to coat the LCN/SF. Interestingly, even after the addition of the sixth layer, there was no significant increase in particle size (Figure 2A). The PDI was found to be the lowest after the final layer was applied to the LCNs, which might have been caused by the compact layering. Figure 2B illustrates the change in ζ potential following the application of each polymer layer. The seesaw-like ζ potential clearly explains the assembly of each layer applied to the LCNs. The charge possessed by the LbL-LCN could provide colloidal stability and the PEG shell could prevent aggregation.[25] Figure 2C shows the effect of polymer layer addition on the EE and LC of SF. Although a slight

DOI: 10.1021/acsami.5b06203
ACS Appl. Mater. Interfaces 2015, 7, 20360−20368

reduction was observed in both parameters during the addition of the polymer layers to LCN, LbL-LCN/SF maintained a high EE.

Characterization of LbL-LCN/SF. TEM images of LCN/SF and LbL-LCN/SF are presented in Figure 3. At lower magnification, cubosomes-like structure formation was evident. The addition of polymer layers induced less staining in the layer around the LCNs, suggesting that the polymer layers were deposited on the LCNs. An increase in the polymer layer coating also increased the layer size. A slight increase in particle size similar to that shown by DLS was evident. Further morphological alterations and polymer layer deposition were confirmed using AFM imaging, and Figure 4 presents the images for LCN/SF and LbL-LCN/SF. Table 1 presents the results of the particle size analyses and height of the LCN/SF and LbL-LCN/SF. The addition of 0, 2, 4, and 6 polymer layers addition showed an increase in both the size and height of LCN, which further confirmed polymer layer deposition on LCNs.

Table 1. Effect of Layer-by-Layer Polymer Assembly on Particle Size and Height of Liquid Crystalline Nanoparticles (LCN)

	DLS	AFM
no. of layers on LCN	particle size (nm)	height (nm)
0	150.5 ± 0.9	12.9 ± 3.8
2	154.4 ± 1.0	16.1 ± 0.2
4	155.1 ± 1.2	20.1 ± 3.3
6	160.2 ± 1.1	24.3 ± 2.2

The FTIR analysis of LCN, SF, LCN/SF, and LbL-LCN/SF is presented in Figure 5A. The blank LCNs showed characteristic peaks at around 1000, 2900, and 3400 cm^{-1} while those of free SF were below 1600 and above 3000 cm^{-1}. The peaks of the incorporated SF in the LCN/SF were not visible. There are two possible explanations for this. The first may be because of incorporation of SF within the hydrophobic core of LCN, and the other reason might be a possible overlap of the SF and LCN peaks. Similarly, the characteristic peaks of polymers were not significant following the addition of PLL and PEG-*b*-PAsp polymer coatings, suggesting that a thin layer was formed above the LCN.

Figure 5B shows the DSC thermograms of monoolein, poloxamer 407, SF, LCN/SF, and LbL-LCN/SF, which provide information on their physical status. The characteristic endothermic peaks of monoolein, poloxamer 407, and SF (37, 56, and 240 °C, respectively) observed were consistent with previous reports.[26,27] Preparation of the LCN formulation obliterated the individual characteristic peaks, suggesting the plasticizing effects of monoolein.[26] The addition of polymer layers to the LCN did not alter the DSC thermograms of the components compared to those of LCN/SF.

The release profile of SF from LCN/SF and LbL-LCN/SF at different pH conditions is presented in Figure 6. Burst release was evident in the first 2 h with all the formulations followed by sustained release for 48 h. LbL-LCN/SF exhibited lower drug release than the LCN/SF did, which might be attributable to polymer layer assembly that controlled the SF release from the LCNs. The result of the in vitro release studied under different pH conditions showed that the release of SF at pH 7.4 was lower than it was at pH 5.5. There are two possible

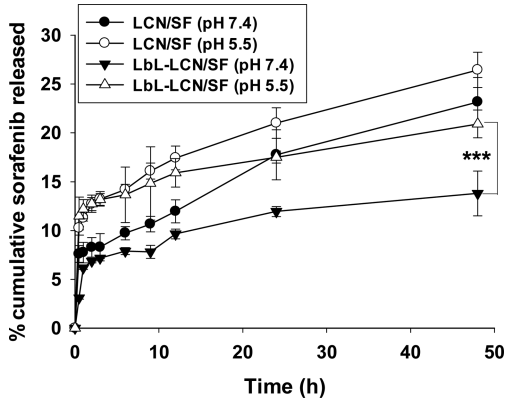

Figure 6. In vitro release profiles of sorafenib (SF) from sorafenib-loaded liquid crystalline nanoparticles (LCN/SF) and layer-by-layer polymer-assembled (LbL)-LCN/SF in physiological (pH 7.4) and acidic (pH 5.0) media at 37 °C. Data are expressed as mean ± SD; n = 3.

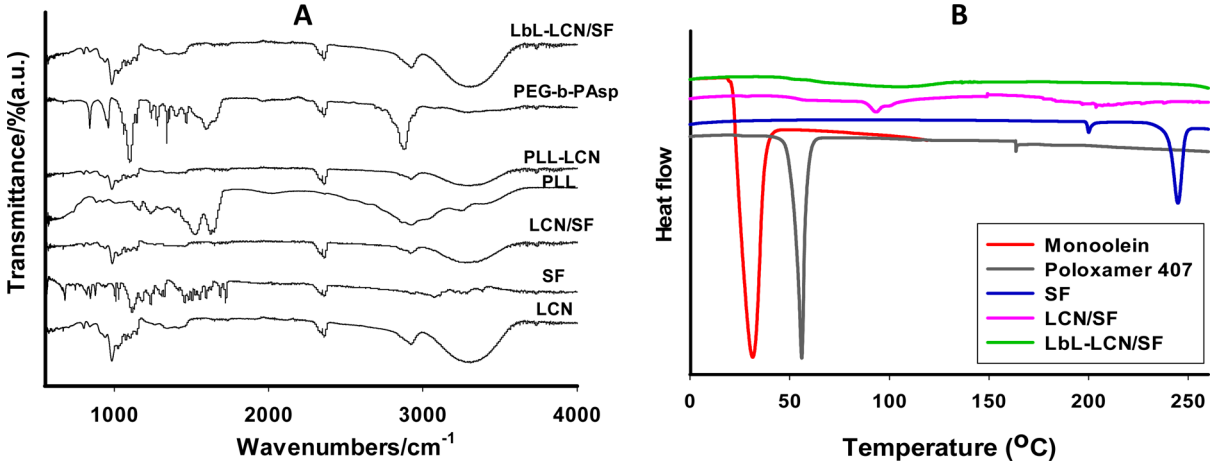

Figure 5. (A) Fourier transform infrared analysis (FTIR) spectra for different liquid crystalline nanoparticle (LCN) formulations. (B) Differential scanning calorimetric (DSC) thermograms of monoolein, poloxamer 407, sorafenib (SF), sorafenib-loaded LCN (LCN/SF), and layer-by-layer polymer-assembled (LbL)-LCN/SF.

DOI: 10.1021/acsami.5b06203
ACS Appl. Mater. Interfaces 2015, 7, 20360−20368

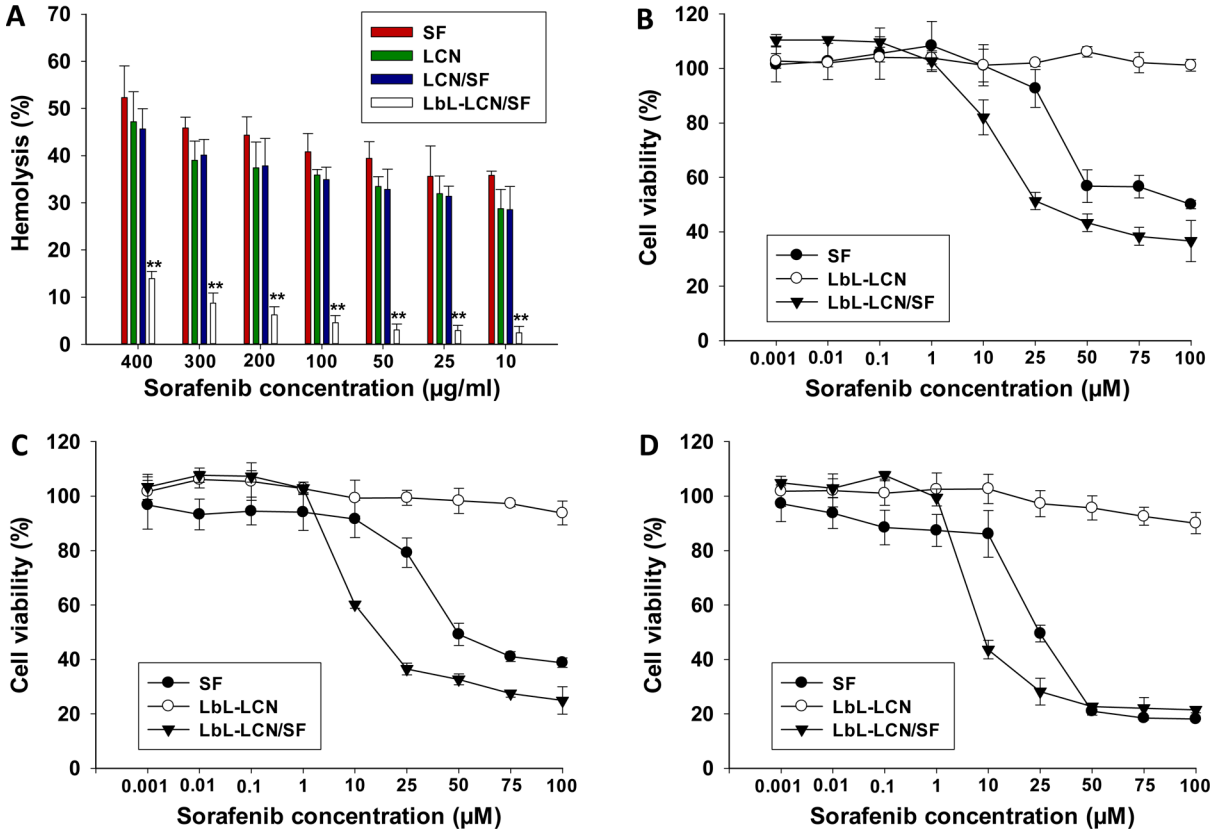

Figure 7. (A) Effects of free sorafenib (SF), blank liquid crystalline nanoparticles (LCN), LCN/SF, and layer-by-layer polymer-assembled (LbL)-LCN/SF on hemolytic toxicity. $^{**}p < 0.01$ compared to free SF; n = three. In vitro cytotoxicity of control (blank LbL-LCN), free SF, and LbL-LCN/SF on HepG2 cell lines following (B) 24, (C) 48, and (D) 72 h incubation. Data are expressed as mean ± SD; n = 8.

explanations for this observation. First, the higher solubility of SF in acidic pH than in normal physiological pH may have contributed. Second, phase inversion of LCN may have occurred, leading to drug leakage from the nanoparticles. Layer-by-layer polymer assembly controls drug release at normal physiological but not acidic pH. However, in acidic pH, LbL-LCN/SF presented a higher drug release than the LCN did. This observation might be due to the disassembly of the polymer layers at acidic pH because of the reduced ionization potential and charge density.[28] A higher drug release at acidic than at physiological pH is beneficial for anticancer effects. This is because tumor microenvironments exhibit acidic conditions at which the nanoparticle would show enhanced release while at normal physiological pH the drug release would slow down.[29]

Hemolytic Toxicity Study. The hemolytic profiles of SF, LCN, LCN/SF, and LbL-LCN/SF at various monoolein concentrations are presented in Figure 7A. The RBC lysis profiles were expressed as a percentage of the hemoglobin released relative to the positive and negative controls. Results suggest that free SF was highly hemolytic. The blank LCNs and LCN/SFs were also highly toxic to RBCs. This hemolytic property poses a constraint to the intravenous delivery of LCNs because it causes irreversible interactions and fusion with the RBC membranes.[13] Therefore, the LCN/SF surface was shielded with PEGylation, which eliminated the potential hemolytic effects of both monoolein and SF by preventing their interaction with the membranes of the RBCs. Multilayering with PEG-*b*-PAsp was found to be highly beneficial in reducing the hemolytic potential of LCN/SF. There was a significant reduction in hemolysis by LbL-LCN/SF compared to LCN/SF ($p < 0.01$). Hemolysis of less than 5% is considered as nontoxic, and LbL-LCN/SF exhibited this property.

In Vitro Cytotoxicity. In vitro cytotoxicity of free SF, blank LbL-LCN, and LbL-LCN/SF against the HepG2 cell line was evaluated at a concentration range of 0.001−100 μM (Figure 7B−D). The results revealed a dose-dependent cytotoxicity for free SF and LbL-LCN/SF, while the blank LbL-LCN exhibited minimal cytotoxic potential. Compared to the free SF, LbL-LCN/SF exhibited a higher cytotoxic potential in HepG2 cells. The half-maximal inhibitory concentration (IC50) values for SF incorporated in LbL-LCN were lower than those of free SF (Table 2). One possible explanation for this observation might be the efflux of free SF from HepG2 cells. Breast cancer receptor protein (BCRP) and adenosine triphosphate (ATP)

Table 2. Half-Maximal Inhibitory Concentration (IC_{50}) Values for HepG2 Cells Following Treatment with Sorafenib (SF) and Layer-by-Layer Polymer-Assembled Sorafenib-Loaded Liquid Crystalline Nanoparticles (LbL-LCN/SF) for 24, 48, and 72 h

	IC_{50} (μM)	
incubation time (h)	SF	LbL-LCN/SF
24	>100	27.82
48	48.30	13.80
72	24.58	7.87

IC_{50} (μM) represents concentration of drug causing 50% inhibition of HepG2 cells in vitro (n = eight)

DOI: 10.1021/acsami.5b06203
ACS Appl. Mater. Interfaces 2015, 7, 20360−20368

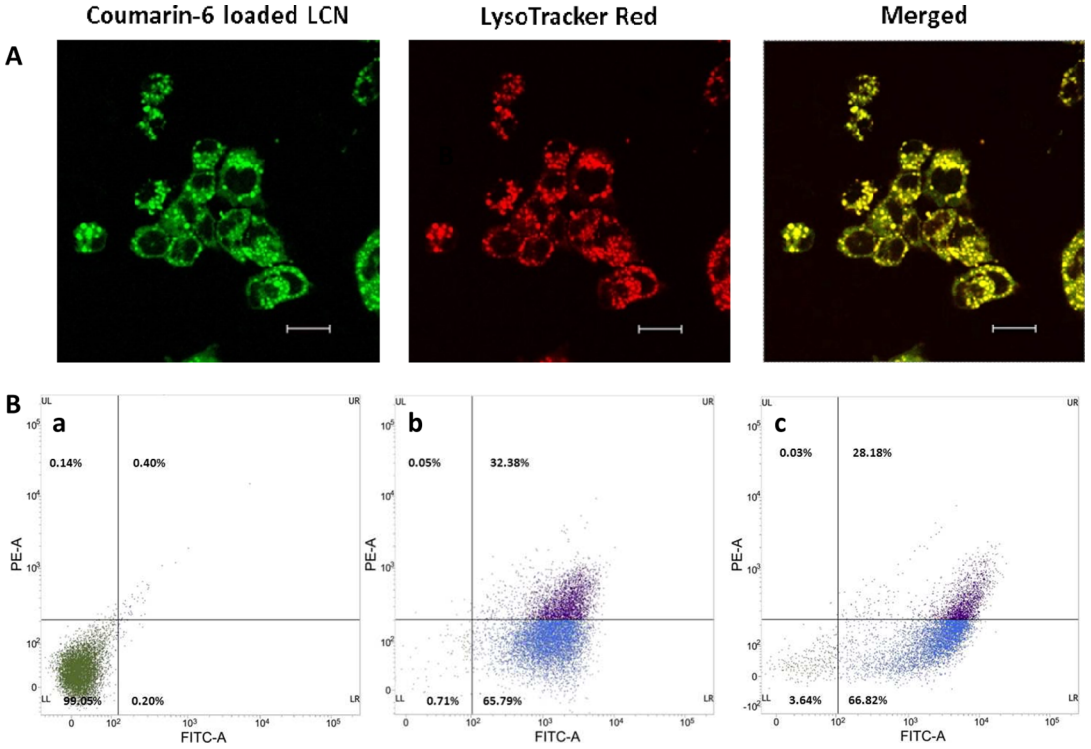

Figure 8. (A) Intracellular uptake of layer-by-layer polymer-assembled liquid crystalline nanoparticles (LbL-LCN) determined by confocal laser scanning microscopy (scale bar, 20 μm). LbL-LCNs containing coumarin-6 (green) and LysoTracker Red (red) were used for the experiment. (B) Fluorescence-activated cell sorting (FACS) analysis of effects of (a) control, (b) free sorafenib (SF), and (c) layer-by-layer assembled (LbL)-LCN/SF on HepG2 cell apoptosis.

binding cassette (ABC) transporter protein (ABCG2) might potentially mediate the SF efflux from HepG2 cells.[30] In contrast, LbL-LCN/SF provide sustained release of SF following its uptake by HepG2 cells, resulting in higher cytotoxicity.

Intracellular Uptake and Apoptosis Study. The intracellular uptake study of LbL-LCN in the HepG2 cell line was performed using FACS. Flow cytometric analysis of coumarin-6-loaded LbL-LCN was performed. The quantitative cellular uptake study revealed a time-dependent cellular uptake of LbL-LCN by HepG2 cells (Figure S3). The qualitative cellular uptake study was performed using confocal microscopy, and Figure 8A shows clear evidence of lysosomal uptake of LbL-LCN into HepG2 cells. Lysosomes exist at pH 4.5−5.0, and, therefore, their cellular uptake of LbL-LCN would create the potential for release of an adequate amount of SF in cancer cells, leading to beneficial antitumor effects.[31]

The apoptosis study of HepG2 cells following treatment with free SF and LbL-LCN/SF is presented in Figure 8B, and the LbL-LCN/SF and free SF induced similar levels of apoptosis. Because the rate of SF release from LbL-LCN/SFs is controlled, they can be expected to show a greater cytotoxicity than that of free SF, following prolonged treatments. Our results demonstrate that LbL-LCN/SF could be superior nanocarriers for the delivery of SF to hepatocellular carcinoma cells.

CONCLUSIONS

In this study, we successfully fabricated LbL-LCN/SF by alternate application of PLL and PEG-*b*-PAsp layers on LCN/SF. Furthermore, the optimized LbL-LCN/SF possessed desirable properties for SF delivery to hepatocellular carcinoma cells. The optimum particle size, PDI, and ζ potential, as well as pH-dependent release profiles, make the LCN/SF favorable for cancer drug delivery. In addition, high cellular uptake and superior apoptotic effects following LbL-LCN/SF treatment suggest that these nanoparticles have the potential to be efficacious formulations for the treatment of hepatocellular carcinoma using SF, with fewer side and unwanted effects.

ASSOCIATED CONTENT

Supporting Information

The Supporting Information is available free of charge on the ACS Publications website at DOI: 10.1021/acsami.5b06203.

Optimization of LCN with different ratios of monoolein/poloxamer 407, poly(vinyl alcohol), ethanol, and sorafenib and FACS analysis of coumarin-6-loaded LbL-LCN in HepG2 cells (PDF)

AUTHOR INFORMATION

Corresponding Authors

*(H.-G.C.) Tel.: +82-31-400-5802. Fax: +82-31-400-5958. E-mail: hangon@hanyang.ac.kr.

*(C.S.Y.) Tel.: +82-53-810-2812. Fax: +82-53-810-4654. E-mail: csyong@yu.ac.kr.

*(J.O.K.) Tel.: +82-53-810-2813. Fax: +82-53-810-4654. E-mail: jongohkim@yu.ac.kr.

Notes

The authors declare no competing financial interest.

ACKNOWLEDGMENTS

This research was supported by the National Research Foundation of Korea (NRF) grant funded by the Korea

DOI: 10.1021/acsami.5b06203
ACS Appl. Mater. Interfaces 2015, 7, 20360−20368

government (MSIP) (Nos. 2015R1A2A2A01004118 and 2015R1A2A2A04004806). This work was also supported by the Medical Research Center Program (Grant 2015R1A5A2009124) through the NRF funded by MSIP.

REFERENCES

(1) Jemal, A.; Bray, F.; Center, M. M.; Ferlay, J.; Ward, E.; Forman, D. Global Cancer Statistics. *Ca-Cancer J. Clin.* **2011**, *61*, 69−90.
(2) El-Serag, H. B. Hepatocellular Carcinoma. *N. Engl. J. Med.* **2011**, *365*, 1118−1127.
(3) Marotta, F.; Vangieri, B.; Cecere, A.; Gattoni, A. The Pathogenesis of Hepatocellular Carcinoma is Multifactorial Event. Novel Immunological Treatment in Prospect. *Clin. Ter.* **2004**, *155* (5), 187−199.
(4) Calvisi, D. F.; Ladu, S.; Gorden, A.; Farina, M.; Conner, E. A.; Lee, J. S.; Factor, V. M.; Thorgeirsson, S. S. Ubiquitous Activation of Ras and Jak/Stat Pathways in Human HCC. *Gastroenterology* **2006**, *130* (4), 1117−1128.
(5) Avila, M. A.; Berasain, C.; Sangro, B.; Prieto, J. New Therapies for Hepatocellular Carcinoma. *Oncogene* **2006**, *25* (27), 3866−3884.
(6) Xie, B.; Wang, D. H.; Spechler, S. J. Sorafenib for Treatment of Hepatocellular Carcinoma: A Systemic Review. *Dig. Dis. Sci.* **2012**, *57* (5), 1122−1129.
(7) Kane, R. C.; Farrell, A. T.; Madabushi, R.; Booth, B.; Chattopadhyay, S.; Sridhara, R.; Justice, R.; Pazdur, R. Sorafenib for the Treatment of Unresectable Hepatocellular Carcinoma. *Oncologist* **2009**, *14* (1), 95−100.
(8) Wang, X. Q.; Fan, J. M.; Liu, Y. O.; Zhao, B.; Jia, Z. R.; Zhang, Q. Bioavailability and Pharmacokinetics of Sorafenib Suspension, Nanoparticles and Nanomatrix for Oral Administration to Rat. *Int. J. Pharm.* **2011**, *419*, 339−346.
(9) Zhang, J. Y.; He, B.; Qu, W.; Cui, Z.; Wang, Y. B.; Zhang, H.; Wang, J. C.; Zhang, Q. Preparation of the Albumin Nanoparticle System Loaded with Both Paclitaxel and Sorafenib and its Evaluation In vitro and In vivo. *J. Microencapsulation* **2011**, *28*, 528−536.
(10) Swarnakar, N. K.; Thanki, K.; Jain, S. Bicontinuous Cubic Liquid Crystalline Nanoparticles for Oral Delivery of Doxorubicin: Implications on Bioavailability, Therapeutic Efficacy, and Cardiotoxicity. *Pharm. Res.* **2014**, *31* (5), 1219−1238.
(11) Yang, D.; Armitage, B.; Marder, S. R. Cubic Liquid-crystalline Nanoparticles. *Angew. Chem., Int. Ed.* **2004**, *43* (34), 4402−4409.
(12) Barauskas, J.; Johnsson, M.; Tiberg, F. Self-assembled Lipid Superstructures: Beyond Vesicles and Liposomes. *Nano Lett.* **2005**, *5* (8), 1615.
(13) Barauskas, J.; Cervin, C.; Jankunec, M.; Spandyreva, M.; Ribokaite, K.; Tiberg, F.; Johnsson, M. Interactions of Lipid-Based Liquid Crystalline Nanoparticles with Model and Cell Membranes. *Int. J. Pharm.* **2010**, *391* (1−2), 284−291.
(14) Gabizon, A.; Shmeeda, H.; Zalipsky, S. Pros and Cons of the Liposome Platform in Cancer Drug Targeting. *J. Liposome Res.* **2006**, *16*, 175−183.
(15) Allen, T. M.; Mehra, T.; Hansen, C.; Chin, Y. C. Stealth Liposomes: An Improved Sustained Release System for 1-beta-D-arabinofuranosylcytosine. *Cancer Res.* **1992**, *52* (9), 2431−2439.
(16) Thapa, R. K.; Yoo, B. K. Evaluation of the Effect of Tacrolimus-loaded Liquid Crystalline Nanoparticles on Psoriasis-like Skin Inflammation. *J. Dermatol. Treat.* **2014**, *25* (1), 22−25.
(17) Thapa, R. K.; Baskaran, R.; Madheswaran, T.; Kim, J. O.; Yong, C. S.; Yoo, B. K. Preparation, Characterization, and Release Study of Tacrolimus-loaded Liquid Crystalline Nanoparticles. *J. Dispersion Sci. Technol.* **2013**, *34* (1), 72−77.
(18) Ramasamy, T.; Haidar, Z. S.; Tran, T. H.; Choi, J. Y.; Jeong, J. H.; Shin, B. S.; Choi, H. G.; Yong, C. S.; Kim, J. O. Layer-by-layer Assembly of Liposomal Nanoparticles with PEGylated Polyelectrolytes Enhances Systemic Delivery of Multiple Anticancer Drugs. *Acta Biomater.* **2014**, *10* (12), 5116−5127.
(19) Agashe, H. B.; Dutta, T.; Garg, M.; Jain, N. K. Investigations on the Toxicological Profile of Functionalized Fifth-generation Poly(propylene imine) Dendrimer. *J. Pharm. Pharmacol.* **2006**, *58*, 1491−1498.
(20) Mayer, A.; Vadon, M.; Rinner, B.; Novak, A.; Wintersteiger, R.; Frohlich, E. The Role of Nanoparticle Size in Hemocompatibility. *Toxicology* **2009**, *258* (2-3), 139−147.
(21) Maeda, H.; Wu, J.; Sawa, T.; Matsumura, Y.; Hori, K. Tumor Vascular Permeability and the EPR Effect in Macromolecular Therapeutics: A Review. *J. Controlled Release* **2000**, *65* (1−2), 271−284.
(22) Choi, J. Y.; Ramasamy, T.; Tran, T. H.; Ku, S. K.; Shin, B. S.; Choi, H. G.; Yong, C. S.; Kim, J. O. Systemic Delivery of Axitinib with Nanohybrid Liposomal Nanoparticles Inhibits Hypoxic Tumor Growth. *J. Mater. Chem. B* **2015**, *3*, 408−416.
(23) Garg, G.; Saraf, S.; Saraf, S. Cubosomes: An Overview. *Biol. Pharm. Bull.* **2007**, *30* (2), 350−353.
(24) Spicer, P. T.; Hayden, K. L.; Lynch, M. L.; Ofori-Boateng, A.; Burns, J. L. Novel Process for Producing Cubic Liquid Crystalline Nanoparticles (Cubosomes). *Langmuir* **2001**, *17* (19), 5748−5756.
(25) Yoon, H. J.; Lim, T. G.; Kim, J. H.; Cho, Y. M.; Kim, Y. S.; Chung, U. S.; Kim, J. H.; Choi, B. W.; Koh, W. G.; Jang, W. D. Fabrication of Multifunctional Layer-by-Layer Nanocapsules Toward the Design of Theragnostic Nanoplatform. *Biomacromolecules* **2014**, *15* (4), 1382−1389.
(26) Bei, D.; Zhang, T.; Murowchick, J. B.; Youan, B. B. Formulation of Dacarbazine-loaded Cubosomes. Part III. Physicochemical Characterization. *AAPS PharmSciTech* **2010**, *11* (3), 1243−1249.
(27) Zhang, H.; Zhang, F. M.; Yan, S. J. Preparation, In vitro Release, and Pharmacokinetics in Rabbits of Lyophilized Injection of Sorafenib Solid Lipid Nanoparticles. *Int. J. Nanomed.* **2012**, *7*, 2901−2910.
(28) Ramasamy, T.; Tran, T. H.; Cho, H. J.; Kim, J. H.; Kim, Y. I.; Jeon, J. Y.; Choi, H. G.; Yong, C. S.; Kim, J. O. Chitosan-based Polyelectrolyte Complexes as Potential Nanoparticulate Carriers: Physicochemical and Biological Characterization. *Pharm. Res.* **2014**, *31* (5), 1302−1314.
(29) Kato, Y.; Ozawa, S.; Miyamoto, C.; Maehata, Y.; Suzuki, A.; Maeda, T.; Baba, Y. Acidic Extracellular Microenvironment and Cancer. *Cancer Cell Int.* **2013**, *13*, 89 (8 pp)..
(30) Huang, W. C.; Hsieh, Y. L.; Hung, C. M.; Chien, P. H.; Chien, Y. F.; Chen, L. C.; Tu, C. Y.; Chen, C. H.; Hsu, S. C.; Lin, Y. M.; Chen, Y. J. BCRP/ABCG2 Inhibition Sensitizes Hepatocellular Carcinoma Cells to Sorafenib. *PLoS One* **2013**, *8* (12), e83627.
(31) Feng, S. T.; Li, J.; Luo, Y.; Yin, T.; Cai, H.; Wang, Y.; Dong, Z.; Shuai, X.; Li, Z. P. pH-sensitive Nanomicelles for Controlled and Efficient Drug Delivery to Human Colorectal Carcinoma LoVo Cells. *PLoS One* **2014**, *9* (6), e100732.

DOI: 10.1021/acsami.5b06203
ACS Appl. Mater. Interfaces 2015, 7, 20360−20368